Hybrid lipid nanoparticles derived from human mesenchymal stem cell extracellular vesicles by microfluidic-sonication for collagen I mRNA delivery to human tendon progenitor stem cells

Pareja Tello, Rubén

Royal Society of Chemistry
2025-04-08

Pareja Tello, R, Lamparelli, E P, Ciardulli, M C, Hirvonen, J, Barreto, G, Mafulli, N, Della Porta, G & Santos, H A 2025, 'Hybrid lipid nanoparticles derived from human mesenchymal stem cell extracellular vesicles by microfluidic-sonication for collagen I mRNA delivery to human tendon progenitor stem cells', Biomaterials Science, vol. 13, no. 8, pp. 2066-2081. https://doi.org/10.1039/D4

http://hdl.handle.net/10138/593063
10.1039/D4BM01405G

Biomaterials Science

Accepted Manuscript

This article can be cited before page numbers have been issued, to do this please use: R. Pareja Tello, E. P. Lamparelli, M. C. Ciardulli, J. Hirvonen, G. Barreto, N. Maffulli, G. Della Porta and H. A. Santos, *Biomater. Sci.*, 2025, DOI: 10.1039/D4BM01405G.

ROYAL SOCIETY OF CHEMISTRY

rsc.li/biomaterials-science

View Article Online
DOI: 10.1039/D4BM01405G

ARTICLE

Hybrid lipid nanoparticles derived from human mesenchymal stem cell extracellular vesicles by microfluidic-sonication for collagen I mRNA delivery to human tendon progenitor stem cells

Received 00th January 20xx,
Accepted 00th January 20xx

DOI: 10.1039/x0xx00000x

Rubén Pareja Tello[a,b,*], Erwin Pavel Lamparelli[b], Maria Camilla Ciardulli[b], Jouni Hirvonen[a], Goncalo Barreto[c,d,e], Nicola Mafulli[f], Giovanna Della Porta[b,g,*], Hélder A. Santos[a,h,*]

Tendon degeneration remains an intricate pathological process characterized by the coexistence of multiple dysregulated homeostasis processes, including the increase in collagen III production in comparison with collagen I. Mesenchymal stem cells-derived extracellular vesicles (MSC-EVs) remain a promising therapeutic tool thanks to their pro-regenerative properties and applicability as drug delivery systems, despite their drug loading limitations. Herein, we developed MSC-EVs derived hybrid lipid nanoparticles (MSC-Hyb NPs) using a microfluidic-sonication technique as an alternative platform for the delivery of collagen type I (COL 1A1) mRNA in pathological TSPCs. The produced MSC-Hyb NPs owned LNPs-like physicochemical characteristics with 178.6 nm size and 0.245 PDI values. Moreover, MSC-Hyb NPs encapsulated mRNA and included EVs-derived surface proteins such as CD63, CD81 and CD144. MSC-Hyb NPs remained highly biocompatible with TSPCs and proved to be functional mRNA delivery agents with certain limitations in comparison with lipid nanoparticles (LNPs). In vitro efficacy studies in TSPCs showed a 2-fold increase in procollagen type I carboxy-terminal peptide production comparable with the effect caused by LNPs. Therefore, our work provides an alternative production method for MSC-EVs derived hybrid NPs and supports their potential use as drug delivery systems for tendon regeneration.

Introduction

Tendinopathies comprise a wide and multi-faceted range of disorders that prevent the ability of the tendon to heal due to chronic deregulation of the tissue homeostasis(1). Current definitions maintain that tendinopathies include different stages starting with a preliminary susceptible phase caused by a wide range of factors, including repetitive loading forces and high levels of oxidative and proinflammatory mediators, among others(2). This initial phase is followed by the activation of multiple dysregulated healing mechanisms causing excessive cellular proliferation and extracellular matrix (ECM) alterations(3–5)

Tendon stem/progenitor cells (TSPCs) refer to a highly heterogeneous cell population isolated from tendon tissue with multipotent differentiation capacity, clonogenicity and self-renewal potential(6), as well as a highly remarkable role in tendon homeostasis and repair (7). Moreover, in vitro gene expression studies have shown that TSPCs can express either adipogenic, chondrogenic or osteogenic differentiation profiles(8). It has been reported that TSPCs from pathological tendons own different morphological properties due to a higher prevalence of disorganized collagen type III fibres and lower presence of collagen type I in comparison with TSPCs isolated from healthy tendons(9). Differences between type I collagen and type III collagen networks constitute fundamental for the maintenance of the tissue mechanical properties, since collagen type III fibrils remain thinner and more extensive than type I collagen fibrils(10). Therefore, recently developed therapeutic strategies focus on enhancing the presence of aligned collagen I fibres and remodelling the tendon ECM(11).

Extracellular vesicles (EVs) remain lipidic bilayer-based vesicles derived from multivesicular bodies(12) that can be classified according to their diameter and their different mechanism of formation(13). EVs have been described to own intrinsic functions as endocytosis mediators and trafficking agents, delivering different cargos including proteins, lipids and coding and non-coding nucleic acids, such as miRNAs and even DNA(14,15). Among the different EVs that have been studied as potential therapeutical agents for the treatment of

[a] Drug Research Program, Division of Pharmaceutical Chemistry and Technology, University of Helsinki, Helsinki FI-00014, Finland.
[b] Department of Medicine, Surgery and Dentistry, University of Salerno, via S. Allende, 84081 Baronissi, SA, Italy.
[c] Clinicum, Faculty of Medicine, University of Helsinki and Helsinki University Hospital, 00014 Helsinki, Finland.
[d] Medical Ultrasonics Laboratory (MEDUSA), Department of Neuroscience and Biomedical Engineering, Aalto University, 02150 Espoo, Finland.
[e] Orton Orthopedic Hospital, Tenholantie 10, 00280 Helsinki, Finland.
[f] Department of Trauma and Orthopaedics, Faculty of Medicine and Psychology, Sant' Andrea Hospital, Sapienza University, 00189 Rome, Italy.
[g] Interdepartment Centre BIONAM, University of Salerno, Via Giovanni Paolo II, 84084 Fisciano, SA, Italy.
[h] Department of Biomaterials and Biomedical Technology, The Personalized Medicine Research Institute (PRECISION), University Medical Center Groningen (UMCG), University of Groningen, Ant. Deusinglaan 1, 9713 AV Groningen, The Netherlands.
* Corresponding author: h.a.santos@umcg.nl
(https://orcid.org/0000-0001-7850-6309)
Supplementary Information available: [details of any supplementary information available should be included here]. See DOI: 10.1039/x0xx00000x

tendinopathies, mesenchymal stem cells-derived EVs (MSC-EVs) have gained the most attention. Firstly, MSCs can be isolated from different source tissues, including adipose tissue or bone marrow, which reduces the numerous ethical concerns associated with other types of cells(16). MSC-EVs have been described as essential paracrine mediators and several studies have proved that they possess immunomodulatory and pro-regenerative properties(17–20). The observed properties do not exclusively require cell-to-cell contact between MSCs and other cells, but rather depend on the secretion of MSC EVs, cytokines and microRNAs, which exert the described effects(21). Therefore, MSC-EVs remain promising therapeutical tools for the treatment of tendinopathies.

Nanoparticle (NP)-based cell systems have high biocompatibility properties(22), aiming to improve biological barriers-crossing capabilities, easing the path to target specific tissues of interest or reducing the immunogenicity in comparison with other synthetic nanosystems(23). Therefore, MSC-EVs own several benefits and constitute highly promising cell-based delivery systems capable of being loaded with additional external molecules(24–26), including proteins, mRNA and siRNA, which can be endogenously loaded(27–30) or exogenously after its formation(31–36). However, EVs' high potential as delivery agents remains highly limited by the low entrapment efficiency (EE) of external molecules in comparison with several other synthetic systems, as well as the limited reproducibility and robustness correlated with their production(37). Consequently, the search for different methods to optimize the loading of additional cargos in EVs remains necessary to enhance and improve the potential of EVs as nanocarriers.

A recently described approach is based on the production of hybrid NPs derived from MSC-EVs and synthetic lipid NPs with the aim to integrate the advantageous properties of both types of systems within a single nanocarrier(38). Hybrid NPs have been described to be produced by the fusion of both MSC-EVs and lipid NPs precursors by different bulk methodologies, such as extrusion or freeze-thawing(39). However, most of these methods are correlated with substantial disadvantages, such as significant alterations of the membrane integrity and even damage of the loaded cargo by either repeated freeze-thaw cycles or the high pressure applied during extrusion.

Herein, we aim to produce MSC-derived hybrid (MSC-Hyb) NPs from adipose tissue-derived MSC-EVs using the microfluidic-sonication technology as an alternative platform for the delivery of mRNA. Microfluidic remains a highly reproducible technique commonly used to produce lipidic NPs (LNPs) and the encapsulation of different types of payloads, such as siRNA and mRNA, with high EE(40–43). MSC-Hyb NPs require the original EVs to disrupt their lipidic structure and subsequently reassemble in the presence of additionally added synthetic lipids to form a hybrid structure combining materials from both origins(44). Previous studies suggest that the combination of sonication with microfluidics allows to exert the required force fields to rupture cellular lipidic membranes within the microfluidic channels, as only hydrodynamic forces are not enough to allow this process(45).

In this work, we focused on the development of MSC-Hyb NPs for the delivery of functional collagen type I (COL 1A1) mRNA in pathological TSPCs. MSC-Hyb were produced and optimized by microfluidic-sonication using a staggered herringbone micromixer structure. The size and morphology of the produced NPs were characterized by dynamic light scattering (DLS), NP tracking analysis (NTA) and cryogenic transmission electron microscopy. Moreover, the encapsulation of the mRNA payload was assessed by the Ribogreen assay and the hybrid nature of the obtained MSC-Hyb NPs was studied by fluorescence resonance energy transfer (FRET) and by surface antigens analysis. Biological in vitro studies were conducted in TSPCs and in a common mammalian immortalized cell model, Chinese hamster ovary (CHO) cells, using enhanced green fluorescence protein (eGFP) mRNA as a cargo model. Cytocompatibility, cell-NP interactions and mRNA transfection efficacy of the system were also studied. Subsequently, NPs were loaded with COL1A1 mRNA and in vitro studies were conducted in human pathological primary TSPCs to assess the production of collagen I after the treatment.

Experimental section

Materials for MSC-Hyb and LNPs preparation

6-((2-hexyldecanoyl)oxy)-N-(6-((2-hexyldecanoyl)oxy)hexyl)-N-(4-hydroxybutyl)hexan-1-aminium (ALC-0315), 18:0 1,2-distearoyl-sn-glycero-3-phosphocholine (DSPC), cholesterol, Methoxypolyethyleneglycoloxy(2000)-N,N-ditetradecylacetamide (ALC-0159), 18:1 1,2-dioleoyl-sn-glycero-3-phosphoethanolamine-N-(lissamine rhodamine B sulfonyl) ammonium salt (Rhodamine-PE), and 18:1 1,2-dioleoyl-sn-glycero-3-phospho-L-serine-N-(7-nitro-2-1,3-benzoxadiazol-4-yl) ammonium salt (NBD-PS) were purchased from Avanti Polar Lipids (Alabama, USA). Lyophilized and purified extracellular vesicles from human mesenchymal stem cells (hMSC) obtained from adipose tissue were purchased from Hansabiomed (Tallinn, Estonia). eGFP mRNA and COL 1A1 mRNA were purchased from Ribopro (Oss, Netherlands). Slide-A-LyzerTM dialysis cassettes 10 kDa were purchased from Thermo Fisher Scientific (Waltham, MA, USA). Quant-itTM RiboGreen RNA assay kit was purchased from Thermo Fisher Scientific (Waltham, MA, USA).

Materials for cell culture

Human primary TSPCs from pathological Achilles tendon were isolated as reported elsewhere(9). The isolation protocol is described in the Supporting Information. TSPCs were used at passages #2–5 in the conducted in vitro studies.

α-MEM (Corning, Manassas, VA, United States) supplemented with 1% GlutagroTM (Corning, Manassas, VA, United States), 10% fetal bovine serum (FBS) (GibcoTM, Walthan, MA, USA), 1% Penicillin/Streptomycin (Corning, Manassas, VA, United States) and 1% Amphotericin B (Corning, Manassas, VA, United States) was used as cell culture medium for TSPCs, which were incubated at 37°C, 5% of CO_2 and 95% relative humidity. The cell medium was changed every 2-3 days. HAM'S F-12 (Corning,

View Article Online
DOI: 10.1039/D4BM01495C

Manassas, VA, United States) supplemented with 10% FBS and 1% Penicillin/Streptomycin was used as the cell culture medium for CHO cells, which were incubated at 37°C, 5% of CO_2 and 95% relative humidity. The cell medium was changed every 2-3 days. Sterile phosphate buffer saline (PBS) 1x (Corning, Manassas, VA, United States) and trypsin-ethylenediamine tetraacetic acid (EDTA, Corning, Manassas, VA, United States) were used for cell subculturing.

Development and purification of MSC-Hyb and LNPs

Empty and mRNA-loaded LNPs were prepared by NanoGenerator Flex (Precigenome LLC San Jose, CA, USA) using a staggered herringbone micromixer chip (Precigenome LLC San Jose, CA, USA). The organic phase contained a lipid mixture including ALC-0315:DSPC:cholesterol:ALC-0159 dissolved in ethanol at a 0.5:0.1:0.385:0.015 molar ratio. To load mRNA, the aqueous phase included either eGFP mRNA or COL 1A1 mRNA immersed in 0.1 M citrate buffer (pH 5), following a N:P ratio of 15:1. Empty and mRNA-loaded MSC-Hyb were prepared with a similar protocol with some additional steps. In this case, EVs from hMSC were resuspended and additionally added to the aqueous phase following weight ratios between EVs and total lipid weight of 1:100, respectively.

For the preparation of both types of formulations, both types of solutions were injected into the chip at a 4 mL/min total flow rate maintaining a 3:1 ratio between the aqueous and the organic phase. The chip was immersed in a sonication bath (FisherbrandTM P-series, 340 x 390 x 321 mm, Elma Schmidbauer GmbH, Germany) under a 30 kHz frequency and 50 W intensity for 1 minute, which was the time the formulation was prepared. Moreover, the sonication bath was maintained at a temperature of 4 ºC to avoid any overheating phenomena(33). The obtained LNPs and MSC-Hyb were purified by dialysis overnight at 4 ºC using Slide-A-Lyzer dialysis cassettes with a membrane cutoff of 10 kDa immersed in PBS 1x to change the pH to 7.4 and separate the non-capsulated mRNA.

Characterization of MSC-Hyb and LNPs

Size, polydispersity index (PDI), and zeta (ζ)-potential analysis: LNPs and MSC-Hyb were characterized by DLS and electrophoretic light scattering (ELS) in terms of average size (Z-average), PDI, and ζ-potential using a Zetasizer Nano ZS instrument 1000HSa (Malvern Panalytical, Malvern, UK) equipped with a He-Ne laser of 633 nm and a detector angle of 173 º. Samples were diluted 1:50 (v/v) with filtered (0.22 µm) Milli-Q water in disposable polystyrene cuvettes (SARSTEDT AG & Co, Germany) in triplicate to determine the size and PDI. Samples were equally diluted in disposable folded capillary cells (DTS1070, Malvern, UK) to determine the ζ-potential.

NTA Analysis: Particle size and concentration of LNPs and MSC-Hyb were measured using NP tracking analysis (NTA) on a NanoSight NS500 (Malvern Panalytical, Malvern, UK) with a sCMOS camera. Samples were diluted 1:1000 (v/v) with filtered (0.22 µm) Milli-Q water to obtain an ideal particle per frame value (20-200 particles/frame). The following settings were set according to the manufacturer: Camera level was increased until clearly visualize particles without exceeding 20% signal saturation, which corresponded to a camera level 12. Five measurements of 1 min were performed under a cell temperature of 25 ºC and pump rate of 30 µL/min. The detection threshold was set for a maximum of 10% non-distinct particles and blue cross count was limited to a maximum of 5 per frame. Moreover, autofocus was adjusted to avoid unclear particles. The recorded videos were analysed using NanoSight Software NTA 3.1 Build 3.1.46 with a sensitivity level of 5.

mRNA quantification and entrapment efficiency (EE) determination

The EE of the loaded LNPs and MSC-Hyb was determined by quantifying the loaded mRNA using Quant-iT RiboGreen RNA Reagent. NPs were dissolved in Triton X-100 (2%, v/v) and incubated during 10 min at 37 ºC to quantify the complexed RNA. Samples were subsequently diluted in TE buffer (1×) to obtain a final Triton X-100 concentration of 0.5%, according to the maximum concentration recommended by the manufacturer. The NPs were simultaneously dissolved in TE buffer (1×) to quantify the non-complexed RNA. The calibration curves of mRNA were prepared in Triton X-100 (0.5%, v/v) and in TE buffer (1×) within a range from 5-1000 ng/mL. The RiboGreen assay was performed following the manufacturer's protocol. The standards corresponding to the calibration curve were resuspended and subsequently 20 µL of each standard were loaded into the wells of the provided 96-well plate. Then, 180 µL of either Triton X-100 (0.5% v/v in TE buffer 1×) or TE buffer (1x) were added. Moreover, volumes of 200 µL from the diluted samples were loaded into the wells of the provided 96-well plate, where the RiboGreen reagent was resuspended by pipetting. The plate was incubated for 10 min in the dark and the concentration of RNA was determined in Nunclon Delta Surface black 96-well plates (ThermoFisher Scientific, Waltham, MA, USA) by fluorescence measurement using a Tecan Infinite® 200 Pro microplate reader (Tecan Trading AG, Switzerland), specifically, with an excitation wavelength of 458 nm and an emission wavelength of 520 nm. The EE was calculated according to Equation (1):

$$EE\ (\%) = \frac{C_{mRNA}\ quantified\ (ng\ mL^{-1})\ x\ V\ (mL)}{Initial\ amount\ of\ mRNA\ added\ (ng)}\ x\ 100\ (1)$$

where C_{mRNA} corresponds to the concentration of mRNA quantified and V corresponds to the volume of sample.

Cryogenic transmission electron microscopy

MSC-Hyb and LPS suspended in RNase free water were vitrified on glow-discharged electron microscopy grids, Quantifoil holey carbon R 1.2/1.3 Cu 300 mesh, using a Leica EM GP plunger at 80% humidity and 1.5 second blotting time using front blotting. Cryo-EM grid screening and data collection were performed at the cryo-EM facility in at the University of Helsinki using a ThermoFisher Scientific Talos Arctica operating at 200 kV and equipped with a Falcon 3 direct electron detector operating in linear mode. Images were collected at 57 k× and 120 k× magnification.

View Article Online
DOI: 10.1039/D4BM01495C

MSC-hybridization studies: FRET analysis and EVs surface marker analysis

The fusion process between the added synthetic lipids and EVs was monitored using a previously described FRET-based lipid mixing assay(46,47). Briefly, LNPs and MSC-Hyb were prepared equally containing a 1.5 molar ratio of two types of lipids conjugated with both donor fluorescent molecules, NBD-PS and Rhodamine-PE. After excitation of NBD at 460 nm, energy is transferred to Rhodamine in a FRET process that mainly depends on the distance between the two fluorophores. Lipid mixing was monitored following the NBD fluorescence intensity, with excitation at 460 nm and emission at 535 nm. The addition of external agents causes the dilution of both fluorophores and an increase on the distance between them within the lipid membrane, causing an increase of NBD fluorescence. Maximum NBD fluorescence intensity was measured after dissolving the obtained LNPs and MSC-Hyb in Triton X-100 1% (w/v) during 10 min at 37 ºC.

To obtain a calibration curve between the percentage of maximal NBD fluorescence and the percentage of addition of external material into the lipid structure, a series of formulations with different amounts of both conjugated lipids were prepared, mimicking an increase in the distance between both fluorochromes. Formulations were prepared with fluorescent lipids ratios of 1.5, 1.3125, 1.125 and 0.75 of donor and acceptor lipids. NBD fluorescence was measured equally using the same total amount of fluorescent lipids in each formulation, i.e., 1.5 ratio (10 µL), 1.3125 ratio (11.43 µL), 1.125 ratio (13.33 µL), 0.75 ratio (20 µL). The value of the non-dissolved standard formulation with 1.5 molar ratio of both conjugated lipids, considered as minimum fluorescence intensity (FI), was subtracted from all the other values, and the change of NBD fluorescence was calculated according to Equation (2):

$$\Delta\, NBD\ (\%) = \frac{[NBD\ FI - Min\ (NBD\ FI)]}{[Max\ (NBD\ FI) - Min\ (NBD\ FI)]}\, x\ 100\ (2)$$

where, NBD FI was the fluorescence measured from a sample, Max (NBD FI) was the maximum NBD fluorescence measured after dissolving the sample in Triton X-100 1% (w/v) during 10 min at 37 ºC, and Min (NBD FI) was the minimum fluorescence intensity from the standard LNPs formulation with lowest NBD signal.

Analysis of EVs surface markers was performed using the human MACSPlex Exosome kit (Miltenyi Biotec, Bergisch-Gladbach, Germany), following the standard short protocol for tubes provided by the manufacturer. Briefly, EVs and MSC-Hybrids (10 µg of protein quantified by MicroBCA), as well as LNPs or PBS as blank control, were diluted in 120 µL of MACSPlex buffer. Samples were incubated with 15 µL capture beads (including all the antibody-coated beads) and 15 µL of detection antibody cocktail (i5 µL of each antibody type including CD9, CD63 and CD81, all conjugated to APC). Samples were mixed and incubated protected from light under agitation for 1h at room temperature. Subsequently, samples were washed twice for 15 min using 0.5 mL MACSPlex buffer and centrifuged at 3000 g for 5 min at room temperature. Finally, samples were measured by BD LSRFortessa™ Cells Analyzer (BD Bioscience, USA) flow cytometry. The results were analysed with FlowJo™ software v.10 (Tree Star, Inc., USA). APC mean fluorescence intensity (MFI) background values corresponding to the PBS blank control were subtracted from each APC MFI value obtained from all the samples.

Cell viability

LNPs and MSC-Hyb were studied in terms of their cytocompatibility in human primary TSPCs and immortalized Chinese Hamster Ovary cells (CHO). Human TSPCs and CHO were seeded in a 96-well plate (Corning, USA) following a density of 5×10^3 cells/cm^2 and 1×10^4 cells/cm^2, respectively, and left to attach overnight. LNPs and MSC-Hyb suspensions at final NPs concentrations of 10, 25, 50, 100, 250 and 500 µg/mL were prepared with cell medium and added to cells, meanwhile cells with Triton X-100 (Merck Millipore, Darmstadt, Germany) were used as positive control and cells with only cell medium were used as a negative control. Cells were incubated at predetermined conditions, 37ºC, 5% CO2 and 5% relative humidity, during two different timepoints of 24 and 48 h. Subsequently, cells were washed twice with Hank's Balanced Salt Solution-(N-[2-hydroxyethyl]piperazine-N'-[2-ethanesulfonic acid]) (HBSS-HEPES, pH 7.4) and immersed in 100 µL CellTiter-Glo®/HBSS-HEPES (1:1). Luminescence was read with a Varioskan™ LUX multimode microplate reader (Thermo Scientific, USA).

Quantitative cellular uptake of rhodamine-labelled MSC-Hyb and LNPs

TSPCs and CHO cells were seeded in 24-well plates at a density of 5×10^3 cells/cm^2 and 1×10^4 cells/cm^2, respectively, and left to attach overnight. Subsequently, rhodamine-labelled MSC-Hyb and LNPs were suspended at the following concentrations: 100 and 200 µg/mL and added to the seeded cells for 24 and 48 h. Afterwards, cells were washed with PBS, detached with trypsin-EDTA, washed twice with PBS and resuspended in 300 µL of PBS. The uptake was analysed by FACS Verse Flow Cytometer (BD FACSVerse, BD Biosciences, IT).

Quantitative transfection efficiency of eGFP mRNA-loaded MSC-Hyb and LNPs

TSPCs and CHO cells were seeded in 24-well plates at a density of 5×103 cells/cm2 and 1×104 cells/cm2, respectively, and left to attach overnight. eGFP mRNA-loaded MSC-Hyb and LNPs were suspended in cell media at the following concentrations: 100 and 200 µg/mL and added to the seeded cells. Cells with only medium were used as negative control and cells with Lipofectamine RNAiMAX at the concentration suggested by the provider were used as positive control. Cells were incubated for 48h and, afterwards, washed with PBS, detached with trypsin-EDTA, washed twice with PBS and resuspended in 300 µL of PBS. The percentage of eGFP-positive cells was measured by FACS Verse Flow Cytometer (BD FACSVerse, BD Biosciences, IT).

View Article Online
DOI: 10.1039/D4BM01495C

Qualitative transfection efficiency and cell uptake of rhodamine-labelled eGFP mRNA-loaded MSC-Hyb and LNPs

Transfection efficiency and labelled NPs uptake were studied by confocal imaging in CHO cells. Cells were seeded on 13 mm^2 coverslips at a density of 1×10^4 cells/cm^2 per well and left to attach overnight. eGFP mRNA-loaded rhodamine-labelled MSC-Hyb and LNPs were suspended in cell media at 200 µg/mL and added to the seeded cells. Cells with only medium were used as negative control and cells with Lipofectamine RNAiMAX at the concentration suggested by the provider were used as positive control. Cells were incubated for 24 and 48h and, afterwards, washed with 1X PBS and fixed with 4% (v/v) paraformaldehyde (PFA) for 30 min at 37 ºC. Samples were washed with 1X PBS and stained with 4',6-diamidino-2-phenylindole (DAPI) at 1 µg/mL for 10 min, followed by three washes with 1X PBS. Finally, image acquisition was at 63x magnification using an inverted Leica laser-scanning confocal microscope (TCS SP5; Leica Microsystems, Wetzlar, Germany) equipped with a plan Apo 63x/1.4 NA oil immersion objective.

Efficacy of COL1A1 mRNA-loaded MSC-Hyb NPs and LNPs in TSPCs

Protein sample preparation: TSPCs were seeded in 6-well plates at a density of 5×10^3 cells/cm^2 and left to attach overnight. Empty MSC-Hyb NPs, empty LNPs, COL1A1 mRNA-loaded MSC-Hyb NPs and COL1AI mRNA-loaded LNPs were added at a concentration of 200 µg/mL for 48 h. Non-treated TSPCs in cell media were used as a negative control. Subsequently, cells were washed with 1X PBS, detached with trypsin-EDTA and washed twice with 1X PBS. Protein extraction from the obtained cell pellet was conducted with RIPA Lysis and Extraction buffer 1X (Thermo Fisher, USA) in combination with 1X Protease and Peptidase Inhibitor cocktail (Thermo Fisher, USA). Samples were incubated on ice for 45 min and centrifuged at 13,000×*g* for 20 min at 4 ºC. Protein lysate supernatants were collected and quantified using micro-BCA assay (Thermo Fisher, USA). A standard curve with different concentrations of BSA within a range between 0–200 µg/mL. Finally, protein samples were prepared by mixing 25 µg of protein with 1X Laemmli buffer and 5% 2-mercaptoethanol to obtain a final volume of 25 µL. Samples were boiled at 95 ºC for 5min.

Gel electrophoresis and western blotting

Gel electrophoresis (Bio-Rad, USA) with 8% nitrocellulose gels (Bio-Rad, USA) was performed by loading 25 µg of each sample and running the gel for 2 h at 80 V. Proteins were transferred to a nitrocellulose membrane (Bio-Rad, USA) using a Turbo Transfer system (Bio-Rad, USA). The membrane was blocked with 10% non-fat dry milk for 1 h at room temperature and incubated overnight at 4 ºC under mild shaking with rabbit anti-human type I collagen antibody (Abcam, ab264074, USA) at 1:1000 in 1X PBS 5% non-fat dry milk and 0.1% Tween-20. A mouse anti-human beta Tubulin (Santa Cruz, sc166729, USA) was used as a lading control at 1:1000. Subsequently, goat anti-rabbit IgG-HRP secondary antibody and goat anti-mouse IgG-HRP (Abcam, USA) were added as secondary antibodies and incubated for 1 h at room temperature under mild shaking. Enhanced chemiluminescence assay (ECL) (Thermo Fisher, USA) was used to develop the membranes using a luminescent image analyser incorporated with a CCD camera (Bio Rad, USA). Quantification of the mean densitometry of the obtained protein bands was performed using ImageJ. Results were normalized to the loading control and expressed as fold change respectively to the untreated samples.

Qualitative study of COL1A1 mRNA-loaded MSC-Hyb NPs and LNPs in TSPCs by immunostaining

TSPCs were seeded on 13 mm^2 coverslips at a density of 5×10^3 cells/cm^2 and left to attach overnight. Empty MSC-Hybs, empty LNPs, COL1A1 mRNA-loaded MSC-Hyb NPs and COL1AI mRNA-loaded LNPs were added at a concentration of 200 µg/mL for 48 h. Non-treated TSPCs in cell media were used as a negative control. Subsequently, cells were washed with 1X PBS, fixed with 3.7% PFA for 30 min at room temperature, permeabilized with 0.1% Triton X-100 for 5 min and blocked with 1% BSA for 1 h. Incubation with mouse monoclonal anti COL1A1 primary antibody (1:100, Sigma-Aldrich, Milan, Italy) was performed overnight at 4 ºC. Afterwards, samples were incubated with DyLight 488 horse anti-mouse IgG (1:500, BioLegend, CA, USA) antibody for 1 h at room temperature. Cell nuclei were stained with DAPI (1:1000) for 5 min. Samples were visualized and image acquisition was performed with an inverted Leica laser-scanning confocal microscope (TCS SP5; Leica Microsystems, Wetzlar, Germany) at 63X magnification and equipped with an Apo 63X/1.4 NA oil immersion objective.

Statistical analysis

Statistical analysis was performed with GraphPad Prism 10 (GraphPad Software, Inc., La Jolla, CA, USA). Each figure includes a complete description of the statistical method used for the analysis of the presented data. The obtained data was predominantly analyzed either by ordinary one-way ANOVA or ordinary two-way ANOVA followed by a Turkey post hoc test.

Ethical permission

Patients involved in the study agreed with their recruitment and sample collection in accordance with the Declaration of Helsinki guidelines by signature of a informed consent, approved by the Institutional Review Board of San Giovanni di Dio e Ruggi D'Aragona Hospital (Salerno, Italy) (Review Board prot./SCCE n. 151 achieved on 29 October 2020).

Results and discussion

LNPs and MSC-Hyb production and physicochemical characterization

The production of EVs-derived hybrid NPs has generally been hypothesized as a highly promising alternative to other drug delivery nanosystems thanks to the combination of intrinsic biological properties and specific targeting capabilities, derived from EVs, with the production reproducibility and high entrapment efficiency of cargos, such as RNA, derived from LNPs(48–50).

View Article Online
DOI: 10.1039/D4BM01405C

Empty LNPs and MSC-Hyb, as well as loaded LNPs and MSC-Hyb encapsulating COL1A1 mRNA, were prepared via microfluidic-sonication with a staggered herringbone micromixer chip(51,52). The use of ultrasound energy remains a highly common methodology used to produce MSC-Hyb NPs, usually in combination with other techniques, such as extrusion(22,53,54). The combined use of microfluidic and sonication has already been previously described as a suitable method to produce MSC-Hyb NPs (NPs) derived from the combination of polymeric NPs and exosomes(45,55). Zhang et al. and Liu et al. described the production of poly(lactic-co-glycolic acid) (PLGA) NPs coated with exosomes-derived membrane in a unique step. The microfluidic setup was immersed in an ultrasonic bath meanwhile the sonication procedure was performed. The application of an external high-frequency sound pressure field allows to surpass the lipid membrane critical compressive stress(56–59) and rupture the exosomes membrane, causing the reassembly of the lipid structures in combination with externally added material.

LNPs and MSC-Hyb were comprised of ALC-0315:DSPC:cholesterol:ALC-0159 following a molar ratio of 0.5:0.1:0.385:0.015 dissolved in ethanol, which constituted the organic phase. Separately, 0.1 M citric buffer (pH 5) was prepared with RNase-free Milli-Q water as aqueous phase. For the preparation of MSC-Hyb, freeze-dried MSC-EVs were added to the aqueous phase considering a crucial parameter, such as the relationship between the amount of EVs used in comparison to the amount of synthetic lipid. Following the reported literature (60,61), different ratios between the amount of protein from EVs and lipid can be found, however, no major indications are reported regarding the number of particles corresponding to the used amount of protein. To assess this, we focused on the use of freeze-dried MSC-derived EVs, which were resuspended in RNase-free Milli-Q water. Subsequently, for the preparation of MSC-Hyb, reconstituted freeze-dried MSC-EVs were added to the aqueous phase following a protein to lipid ratio of 1:100 (w/w). NTA analysis was conducted through the different aqueous phases to study the number of EV particles that were used, and similar values of particles concentration was determined, with an average particle concentration of 2.00×10^{10} particles/mL (**Figure S1**).

Additionally, both types of NPs were loaded with either eGFP mRNA or COL 1A1 mRNA by addition to the aqueous phase at pH 5 of the corresponding amount of mRNA following an N:P ratio of 15:1. The total flow rate and the ratio between the aqueous and organic phases were 4 mL/min and 3:1, respectively, following previously optimized procedures to produce LNPs (62). Both types of samples were purified by dialysis against an excess of 1X PBS overnight to change the pH to 7.4 and, subsequently, their physicochemical properties were studied. Following DLS analysis, **Figure 1A** shows the average size of LNPs and MSC-Hyb, which corresponded to 168.7 nm and 178.6 nm, respectively. Moreover, LNPs and MSC-Hyb measurements indicated PDI values (**Figure 1B**) of 0.135 and 0.245, respectively, indicating that MSC-Hyb owned higher average size and PDI values. ELS analysis revealed that the ζ-potential (**Figure 1C**) of LNPs and MSC-Hyb was -2.15 and -19.5 mV, respectively, revealing a considerable difference of surface charge between both types of samples. The change on ζ-potential might be attributed to the addition of EV membrane into MSC-Hyb, considering EVs prevalently own a negative surface charge.

Regarding the mRNA EE (**Figure 1D**) of both LNPs and MSC-Hyb, Ribogreen assay-mediated quantification of encapsulated mRNA revealed EE values of 71.46% and 51.45% for LNPs and MSC-Hyb, respectively. A decrease in the amount of encapsulated mRNA was observed in MSC-Hyb, which has previously been correlated with the presence of several negatively charged components like RNA, proteins or lipids derived from EVs, which compete with the added mRNA and interact with the used ionizable lipid during the described 1-step production method(54). With the aim to improve the mRNA EE of MSC-Hyb NPs, further studies could focus on the possibility of producing MSC-Hyb based on a 2-step approach, following the initial production of LNPs and, subsequently, the formation of MSC-Hyb NPs after being immersed with EVs under the described sonication parameters, instead of the simultaneous use of microfluidics and sonication. Nevertheless, the obtained EE suggests the capability of the used method to encapsulate mRNA inside MSC-Hyb NPs, indicating that MSC-Hyb NPs are potential mRNA delivery systems. Further

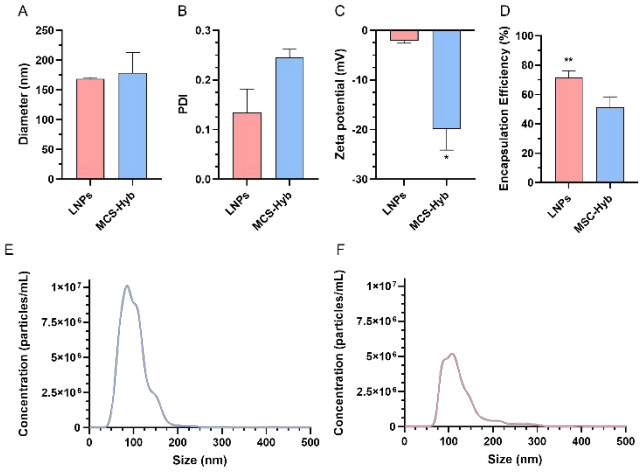

Figure 1. Physicochemical characterization of MSC-Hyb and LNPs. **(A)** Average diameter of MSC-Hyb and LNPs as measured by dynamic light scattering. **(B)** PDI of MSC-Hyb and LNPs as measured by DLS. **(C)** Surface charge (z-potential) of MSC-Hyb and LNPs as measured by dynamic light scattering. **(D)** mRNA encapsulation efficiency of MSC-Hyb and LNPs. **(E)** Size and particle concentration of LNPs determined by NTA. **(F)** Size and particle concentration of MSC-Hyb determined by NTA. Results are presented as mean ± SD (n≥3) and samples were analysed with a paired Student's t-test.

Additional NTA analysis (**Figure 1E-F**) revealed an average size of 106 nm in the case of LNPs and 126.6 nm in the case of MSC-Hyb, which remain slightly lower values in comparison with those obtained by DLS. The slightly different values obtained can be explained by the differences between both techniques. Moreover, considering that both samples were equally diluted 1:1000, the measured sample concentrations were respectively

View Article Online
DOI: 10.1039/D4BM01405G

6.80×10^{11} particles/mL for LNPs and 3.70×10^{11} particles/mL for MSC-Hyb. This confirms that the used microfluidic-sonication technique allows to obtain a significant particle concentration despite the limited initial total lipid and EVs concentration. Interestingly, LNPs were correlated with a higher particle concentration, meanwhile MSC-Hyb showed a lower particle concentration similar to the initial particle concentration of EVs.

Cryo-electron microscopy (Cryo-EM) studies (**Figure 2A-B**) were also conducted on LNPs and MSC-Hyb to confirm the size and size polydispersity data obtained by DLS and NTA. Cryo-EM images revealed that both types of particles owned spherical shape and unilamellar structure, as reported for LNPs and EVs elsewhere(63,64). Moreover, the obtained images confirmed the size and size PDI described by DLS, including slightly smaller and more homogenous LNPs in comparison with MSC-Hyb. MSC-Hyb showed slightly higher size and polydispersity properties, which may be explained by the non-regular incorporation of membrane segments derived from EVs.

To study the MSC-Hyb nature of the produced NPs, FRET-based lipid mixing assay was performed. As it has been previously reported (47,65), fluorescent label-conjugated lipids, NBD-PS and Rhodamine-PE, can be used to study any changes in the lipid membrane thanks to the interaction between NBD, with an excitation wavelength of 460 nm, and Rhodamine, which receives fluorescence resonance energy from NBD depending on the distance between both fluorochromes. The assay allows to detect changes in the distance between both lipids within the lipid membrane after the addition of external components, since the emission of NBD at 535 nm increases substantially due to the dilution of both fluorophores and, therefore, the lack of interaction with nearby Rhodamine molecules. As it is shown in **Figure 2C**, after producing the MSC-Hyb formulation with a 1.5 molar ratio for both labelled lipids, the detected NBD fluorescence increase for the developed formulation was 62.34%. Following the conversion between the increase of NBD fluorescence and the hypothetical round of fusion (**Figure S2**), MSC-Hyb were correlated with a percentage of external material corresponding to 28.99%.

Moreover, we also assessed the presence of EVs' surface markers on the surface of MSC-Hyb NPs using a bead-based flow cytometry analysis tool, MACSPlex Exosome kit, capable of detecting several antigens. Several studies have reported the presence of specific antigen proteins on the surfaces of MSC-derived EVs, including CD81, CD69, which are highly common protein markers detected in EVs (66,67), and CD105 and CD44, highly expressed by MSC (18,68). Bead-based analysis revealed that MSC-Hyb show significant levels of these four proteins in comparison with LNPs (**Figure 2D**), confirming the presence of EVs-derived membrane fragments in the structure of MSC-Hyb NPs. Moreover, MSC-Hyb NPs showed significantly lower levels of these four antigens in comparison with the original EVs, confirming a limited presence of EVs-derived material in MSC-Hyb NPs. Overall, the obtained results prove that the obtained MSC-Hyb NPs were detected by antibody-coated beads against specific EV antigens, confirming that MSC-Hyb NPs contain EVs-derived fragments, which maintain a limited degree of the original surface topology.

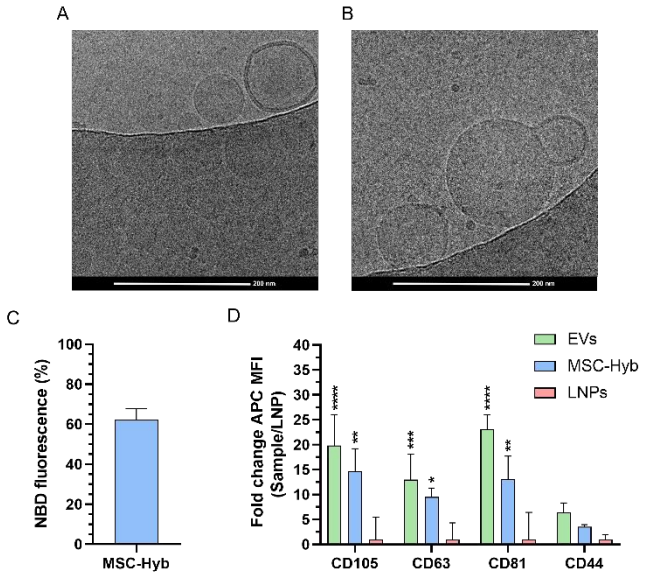

Figure 2. (A-B) Cryo-EM images reveal the morphological characteristics of **(A)** LNPs and **(B)** MSC-Hyb. The highlighted scale bar in both images corresponds to 200 nm. **(C)** FRET studies. NBD fluorescence increase in MSC-Hyb. **(D)** Analysis of EVs surface markers via MACSPlex Exosome kit in EVs, MSC-Hyb and LNPs targeting CD105, CD63, CD81 and CD44. APC MFI background values from PBS blank control were subtracted from each APC MFI value obtained from all the samples and results were represented as fold change relative to LNPs. Results are presented as mean ± SD (n≥3), and the samples were analysed with ordinary one-way ANOVA, followed by Turkey post-hoc test, setting the probabilities *p< 0.05, **p< 0.01, *** p < 0.001, **** p < 0.0001, comparing each EVs and MSC-Hyb sample with the corresponding LNPs sample.

Cell viability studies

The cell viability of LNPs and MSC-Hyb was studied in human primary tendon progenitor stem cells (TSPCs) and in a common epithelial-like mammalian immortalized *in vitro* cell line model, Chinese hamster ovary cells (CHO). Cell viability was assessed using an adenosine triphosphate (ATP)-luciferase based method, CellTiter-Glo luminescence assay(69,70). Cells were exposed to different concentrations of both types of formulations, including 10, 25, 50, 100, 250 and 500 µg/mL, during incubation times of 24 and 48 h. Moreover, both types of cells in their respective cell media were used as negative controls to determine a reference value of 100% cell viability. The obtained results (**Figure 3A-D**) indicated that both formulations owned high biocompatibility with both cell types, since no statistically significant differences were observed between the negative control and the different concentrations at 24 and 48 h, including the highest concentration at 500 µg/mL. Moreover, no major statistically significant differences at each specific concentration were observed between LNPs and MSC-Hyb, except for the two highest concentrations, 250

View Article Online
DOI: 10.1039/D4BM01405G

and 500 µg/mL, after 24 h (**Figure 3A**) of exposition to TSPCs. In these specific conditions, MSC-Hyb NPs showed higher cell viability values in comparison with LNPs, despite no statistically significant differences we observed after 48 h of exposition. This can be explained by the fact that LNPs can slightly compromise the cell viability of TSPCs after shorter exposition times in comparison with MSC-Hyb, but subsequently, after more prolonged exposition times, the effect of LNPs in cell viability is no longer noticeable due to high cell proliferation after extended timepoints.

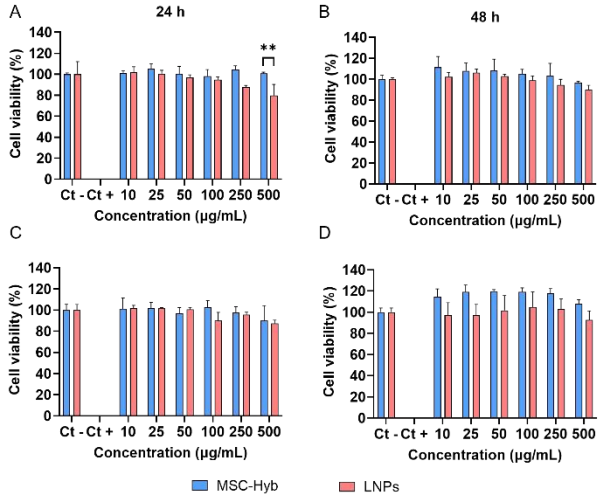

Figure 3. (A-B) Cell viability of TSPCs incubated with MSC-Hyb and LNPs determined by CellTiter assay. Cells were incubated with MSC-Hyb and LNPs at different concentrations from 10 to 500 µg/mL and cell viability was studied after 24 and 48 h. **(C-D)** Cell viability of CHO incubated with MSC-Hyb and LNPs determined by CellTiter assay. Cells were incubated with MSC-Hyb and LNPs at different concentrations from 10 to 500 µg/mL and cell viability was studied after 24 and 48 h. Results are presented as mean ± SD (n≥3), and the samples were analysed with ordinary two-way ANOVA, followed by Turkey post-hoc test, setting the probabilities *p< 0.05, **p< 0.01, comparing each MSC-Hyb and LNPs sample with the untreated cells as well as each MSC-Hyb sample with the equivalent concentration LNPs sample.

Quantitative cell uptake studies

Following the study of the cell biocompatibility of MSC-Hyb and LNPs, we assessed the interaction between both types of NPs and both cell types, CHO and TSPCs, by quantitatively studying the cellular internalization efficiency of both formulations, considering cell internalization remains a critical step for the cytoplasmatic delivery of mRNA. Both types of NPs, LNPs and MSC-Hyb, were produced using Rhodamine-PE, which can be excited by a 546 nm laser and emit fluorescence at 567 nm. Based on the obtained cell viability studies results, we studied the exposure of different concentrations of particles that were correlated with high cell viability values, including 100 and 200 µg/mL. LNPs and MSC-Hyb were incubated with both types of cells for 48 h and, therefore, samples were analyzed by flow cytometry. **Figure 4A-B** shows that cell uptake of MSC-Hyb NPs was statistically significant decreased in comparison with LNPs in both cell types, CHO and TSPCs, after 48 h of incubation. Both MSC-Hyb NPs and LNPs showed a dose-dependent uptake behaviour in CHO cells, which showed a significant internalization degree, 31.53 and 48.85 mean fluorescence intensity (MFI) fold change, after incubation with 100 µg/mL of either MSC-Hyb NPs or LNPs, respectively. The increase of dose to 200 µg/mL of both types of NPs showed a slightly increased internalization degree up to 35.9 and 46.03 MFI fold change correspondingly to MSC-Hyb NPs and LNPs. Moreover, TSPCs similarly showed a dose-dependent uptake behaviour with lower internalization degrees, with MFI fold change values of 31.61 and 53.96 after incubating with 100 µg/mL of MSC-Hyb NPs and LNPs, as well as 60.53 and 89.12 MFI fold change values after incubating with 200 µg/mL of both types of NPs for 48 h. It is important to notice that TSPCs showed a statistically significant fold change increase for both types of NPs in comparison with CHO cells, implicating that cellular internalization of both types of NPs differs between different cell types.

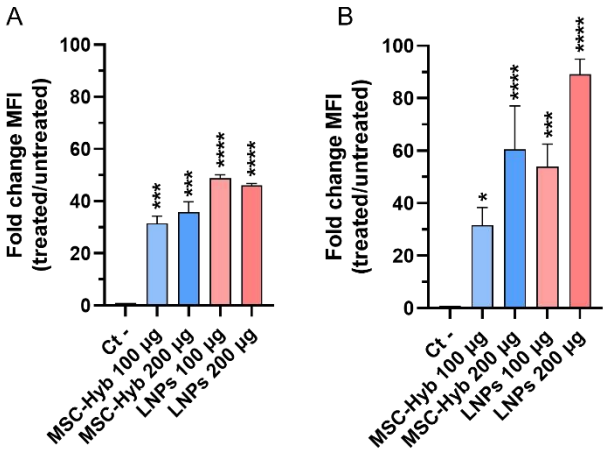

Figure 4. Quantitative cell uptake studies on CHO and TSPCs using flow cytometry. **(A)** CHO were incubated for 48 h at 37ºC with 100 and 200 µg/mL of Rhodamine-PE labelled MSC-Hyb NPs and LNPs. **(B)** TSPCs were incubated for 48 h at 37ºC with 100 and 200 µg/mL of Rhodamine-PE labelled MSC-Hyb NPs and LNPs. Results are represented as mean ± SD (n ≥ 3), and the data was analyzed with ordinary one-way ANOVA, followed by a Turkey post-hoc test, setting the probability at * p < 0.05, ** p < 0.01, *** p < 0.001, **** p < 0.0001, comparing each condition with the negative control.

It has been widely described that NPs cellular internalization can be mediated by different endocytosis processes, which can be easily conditioned by the physicochemical properties of each NP formulation, including size and ζ-potential. Moreover, cellular uptake can also be influenced by the presence of specific biological moieties on the surface of a specific NP's system. The lower internalization rates of MSC-Hyb NPs in comparison with LNPs may be explained by the different physicochemical properties between both types of NPs, especially regarding the size and the surface charge of both NPs, considering MSC-Hyb NPs own a more negative surface charge,

as many other EVs-based NP systems. It has been previously described that EVs can show different uptake ratios comparison with other lipid-based systems. In this case, despite the presence of specific antigens on the surface, the predominant negative charge of MSC-Hyb NPs reduced to a certain extent the number of electrostatic interactions with the negatively charged membrane of both types of cells. Nonetheless, MSC-Hyb NPs still showed high cell uptake rates and proved to be promising NPs-based systems for intracellular delivery.

Quantitative transfection efficiency studies

Subsequently, we evaluated the use of MSC-Hyb NPs and LNPs for the functional delivery of mRNA following the previously described cell uptake studies. To do so, we assessed the efficiency of both MSC-Hyb and LNPs in terms of cytoplasmatic delivery of mRNA, which previously requires endosomal escape of the mRNA cargo after NPs uptake. eGFP mRNA was used as a model mRNA cargo for studying the transfection efficiency of both MSC-Hyb NPs and LNPs in CHO, since it remains a common *in vitro* model to determine the transfection efficiency of LNPs during the initial formulation development phase, as well as in TSPCs. **Figure 5A-B** supports that CHO incubation with 100 and 200 µg/mL MSC-Hyb NPs showed eGFP MFI fold change values of 5.57 and 9.18 (**Figure 5A**), significantly lower in comparison with eGFP MFI fold change values obtained after incubation with 100 and 200 µg/mL of LNPs, which were found to be 76.21 and 77.10, respectively. Furthermore, TSPCs incubation with 100 and 200 µg/mL of eGFP mRNA-loaded MSC-Hyb NPs induced an increase in the percentage of eGFP positive cells of approximately 17.72% and 21.49%, statistically significantly lower to the 85.49% and 78.47% (**Figure 5B**) observed after the incubation with 100 and 200 µg/mL of LNPs.

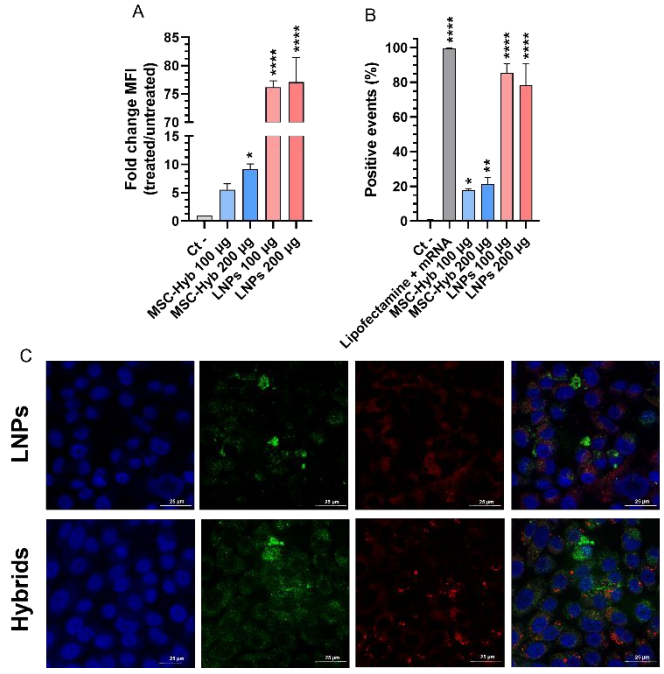

Figure 5. Transfection efficiency of eGFP mRNA-loaded MSC-Hyb and LNPs in **(A-C)** CHO and **(B)** TSPCs cells after 48 h. Both CHO and TSPCs cells were incubated for 48 h at 37ºC with 100 and 200 µg/mL of MSC-Hyb and LNPs and, subsequently, transfection efficiency was assessed by flow cytometry analysis. **(A)** eGFP mean fluorescence intensity in CHO cells represented as fold change relative to the negative control. **(B)** Percentages of eGFP positive TSPCs. Results are represented as mean ± SD ($n \geq 3$), and the data was analyzed with ordinary one-way ANOVA, followed by a Turkey post-hoc test, setting the probability at * $p < 0.05$, ** $p < 0.01$, *** $p < 0.001$, **** $p < 0.0001$, comparing each condition with the negative control. **(C)** Confocal imaging of cellular uptake and eGFP expression of Rhodamine-PE labelled eGFP mRNA-loaded MSC-Hyb and LNPs in CHO cells. Cells were incubated for 48 h at 37ºC with 200 µg/mL of MSC-Hyb and LNPs and imaged using confocal microscopy. MSC-Hyb and LNPs were stained with Rhodamine-PE (red channel), while cells were stained with DAPI (nuclei, blue channel) and the expression of eGFP mRNA was observed using the eGFP channel (green channel).

Overall, MSC-Hyb NPs showed a reduced efficacy in the delivery of mRNA in comparison with LNPs in both cell types. The decrease in the percentage of eGFP positive cells and the degree of eGFP expression can either be explained by the lower uptake degree of MSC-Hyb in comparison to LNPs, as well as the statistically significantly lower mRNA encapsulation efficiency in MSC-Hyb. Therefore, the obtained results indicate that MSC-Hyb NPs are suitable for the delivery of functional mRNA in CHO model cell line and TSPCs primary cells with decreased transfection efficiency in comparison with synthetic LNPs. Considering the previously showed data, including cell viability, quantitative cell uptake and transfection efficiency studies, a concentration of 200 µg/mL for both MSC-Hyb NPs and LNPs was chosen as the appropriate concentration for the following *in vitro* efficacy studies based on the observed safety profile and its transfection efficiency.

Qualitative cell uptake and transfection efficiency studies were performed in CHO cells by incubating the cells with Rhodamine-PE labelled and eGFP mRNA-loaded MSC-Hyb NPs and LNPs. After the incubation with each type of formulation, samples were imaged with confocal microscopy. **Figure 5C** corresponds to single CHO cells and larger cell population images after incubating with MSC-Hyb NPs and LNPs. The images confirm the internalization of MSC-Hyb NPs and LNPs and the expression of eGFP, proving that both types of NPs are suitable for the delivery of mRNA. These results support the obtained data regarding the quantitative uptake studies and the transfection efficacy studies.

Efficacy studies of COL1A1 mRNA-loaded MSC-Hyb NPs and LNPs

TSPCs extracted from pathological tendons have been described to increase the production of collagen type III fibres, which deposit in a disorganized manner during the initial stages of tendon healing. However, the production of collagen I remains low in comparison with non-pathological tendons (71,72). The production of collagen type I is commonly considered a crucial process since the deposition of organized collagen I fibers within tendon bundles allows to improve the tissue mechanical properties and reduce tissue adhesion (73). However, studies suggest that enhancement of collagen I production alone does not correlate with higher ECM regeneration, since it needs to be combined with specific

View Article Online
DOI: 10.1039/D4BM01405G

mechanical stimuli (74,75). Traditionally, numerous studies have focused on the effect on collagen I production caused by administration of growth factors and stem cells-derived culture media (76,77), as well as by stimulation by mechanical stress conditions in combination with bioengineered materials and different *in vitro* culture models (78). However, an alternative approach based on the enhancement of collagen I production via COL1A1 mRNA administration to the affected TSPCs has been previously considered(79,80).

Therefore, after studying the capability of MSC-Hyb NPs to deliver functional mRNA, we assessed the in vitro potential of MSC-Hyb NPs as COL1A1 mRNA delivery agents for pathological TSPCs. TSPCs were treated with COL 1A1 mRNA-loaded MSC-Hyb NPs and LNPs, as well as with empty MSC-Hyb NPs and LNPs, maintaining a NP concentration of 200 µg/mL for 48 h. Moreover, non-treated TSPCs immersed in cell culture medium were used as negative control. Subsequently, collagen I production was assessed by quantitative western blot analysis, as well as qualitative immunofluorescence studies. Figure 6A-C shows protein expression of alpha-1 collagen I from TSPCs from three different donors after incubation with the different treatment groups and analyzed by Western blot. Two predominant and distinctive bands were observed around 180 kDa and 35 kDa, respectively, corresponding to the procollagen alpha-1 chain and procollagen type I carboxy-terminal peptide (PICP)(81). Analysis of the procollagen alpha-1 chain band did not reveal significant differences between the different groups treated with either mRNA-loaded or empty MSC-Hyb and LNPs, possibly due to the already considerable basal expression of procollagen collagen alpha-1 chain in non-treated TSPCs. Nevertheless, analysis of the PICP band revealed a statistically significant increase in TSPCs treated with mRNA-loaded LNPs and MSC-Hyb NPs, with 1.96 and 1.92 relative fold change values, respectively.

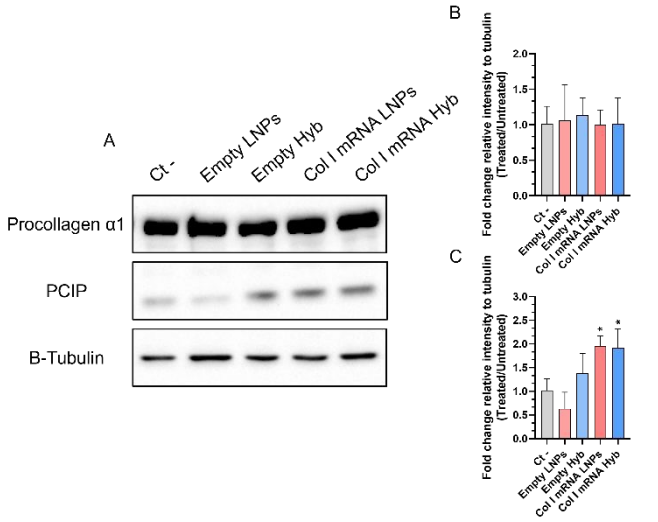

Figure 6. (A) Protein expression analysis by Western Blot of collagen type I in TSPCs to assess the effect of COL1A1 mRNA-loaded MSC-Hyb and LNPs. TSPCs were incubated during 48 h with empty LNPs, empty MSC-Hyb, Col 1A1 mRNA-loaded LNPs and Col I mRNA-loaded MSC-Hyb before proceeding with cell lysis and protein extraction. Western Blot bands are shown, including procollagen α1 and PCIP, as well as β-Tubulin, used as housekeeping protein. **(B)** Densitometric analysis of procollagen α1 expression normalized to β-Tubulin and represented as fold change values relative to the negative control. **(C)** Densitometric analysis of PCIP expression normalized to β-Tubulin and represented as fold change relative to the negative control. Results are represented as mean ± SD (n ≥ 3), and the data was analysed with ordinary one-way ANOVA, followed by a Turkey post-hoc test, setting the probability at *p < 0.05, comparing each condition with the negative control.

Collagen type I owns a triple-helical structure with terminal globular propeptide domains, including both amino and carboxy-ended domains. Specifically, procollagen type I owns a heterodimeric structure based on two α1 chains and one α2 chain assembled as a trimeric structure shortly after their secretion (82). Assembly of this trimeric structure requires endopeptidase-mediated cleavage of each chain at specific amino and carboxy terminal sites. Therefore, three different fragments are generated: collagen type I, which forms collagen fibrils that form the ECM, and two released procollagen type I terminal peptides, one with an amino terminal (PINP) and one with a carboxy terminal (PICP)(83). Different studies report that detection of PICP production remains a suitable marker to study the production of collagen type I in different tissues with a high expression of collagen type I, including bone and skin (84,85). For example, detection of PICP in fibroblasts, either in cell extracts or culture supernatants, has commonly been considered an efficient method to study the production of collagen type I (86,87). Therefore, the significant increase in the production of PICP in TSPCs treated with mRNA-loaded MSC-Hyb and LNPs seems to indicate that MSC-Hyb NPs are equally capable of delivering functional mRNA as LNPs. Additionally, the increase of PICP expression is also statistically significant different in comparison with empty LNPs, which decreased the levels of PICP. Interestingly, empty MSC-Hyb NPs slightly increased PCIP production in comparison with empty LNPs. Despite the increase was found to be non-significant, this may be explained due to the partial EV content of MSC-Hyb NPs, since studies performed with MSC-EVs in tenocytes show a significant increase in collagen type I production (88,89).

Qualitative analysis of collagen type I production in TSPCs was also performed by collagen I immunostaining a confocal microscopy imaging. Figure 7 shows representative images of the collagen I immunostaining in TSPCs after incubating the cells with a concentration of 200 µg/mL of MSC-Hyb and LNPs for 48 h. Images suggest that TSPCs treated with MSC-Hyb and LNPs experience a certain increase in collagen type I in comparison with non-treated TSPCs.

Therefore, the obtained data regarding protein production suggests that MSC-Hyb can act as an equally functional platform as LNPs for the delivery of mRNA in TSPCs, confirming the in vitro potential of MSC-Hyb NPs as COL1A1 mRNA delivery agents for pathological TSPCs.

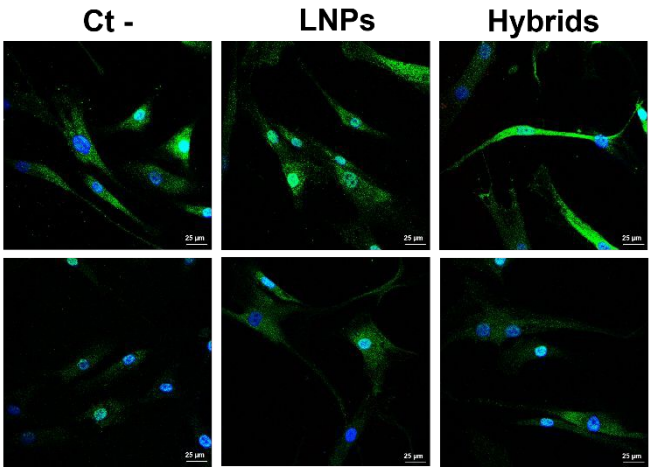

Figure 7. Immunofluorescence staining confocal fluorescence microscope images of collagen type I in 2D cultured TSPCs treated with COL1A1 mRNA-loaded LNPs for 48 h. TSPCs were treated with 200 and 500 µg/mL of COL1A1 mRNA-loaded LNPs and MSC-Hyb for 48 h. Collagen type I was stained using an anti-collagen type I antibody and an Alexa 488-conjugated secondary antibody (green). DAPI was used to stain the nuclei (blue).

Conclusions

Here we combined microfluidic-sonication as an alternative method to produce MSC-EVs derived hybrid NPs encapsulating mRNA. The developed MSC-Hyb NPs owned moderately higher size and PDI values, 178.6 nm and 0.245 respectively, more negative ζ-potential, -19.5 mV, and reduced mRNA EE in comparison with standard LNPs. The conducted physicochemical and EVs-derived surface antigens analysis confirmed the hybrid nature of the produced NPs, which showed the presence of EVs-derived surface proteins, including CD63, CD81 and CD105. Furthermore, MSC-Hyb NPs were found to be highly biocompatible and did not significantly reduce human TSPCs viability even after incubation with the highest concentration of 500 µg/mL. Despite reduced internalization rates and mRNA transfection efficacy in comparison with LNPs, MSC-Hyb NPs remained feasible agents for the internalization and cytoplasmatic delivery of functional mRNA. Moreover, MSC-Hyb NPs were functional for the delivery of COL1A1 mRNA to TSPCs, since their exposition to TSPCs caused a 2-fold increase in procollagen type I carboxy-terminal peptide production, similarly to LNPs. However, despite the efforts, the production of EVs-derived hybrid NPs remains a challenging task mainly due to the limited available knowledge regarding EVs composition and its impact on the development of hybrid NPs, as well as the limited tools available to fully characterize the conformation and structure of hybrid NPs. More in-depth studies will help to gain a better understanding of the observed limitations regarding the loading of mRNA-based cargos or reduced cell internalization, as well as improve the drug delivery capabilities of the described nanosystems.

Author contributions

R.P.T., G.D.P., H.A.S. designed the research. R.P.T., E.P.L., M.C.C. and P.S. performed the research and participated in the discussion of the results. J.H., G.B., N.M., G.D.P and H.A.S. supervised the work and secured the funding for the research work. R.P.T. analyzed the data and wrote the first draft of the publication. All the authors have revised the manuscript and given approval to the final version of the manuscript.

Conflicts of interest

There are no conflicts to declare.

View Article Online
DOI: 10.1039/D4BM01405G

Acknowledgements

This project has been funded thanks to the European Union's Horizon 2020 research and development programme under the Marie Skłodowska Curie grant agreement No. 955685. Additional partial funding was obtained from RNA & Gene Therapy National Research (Next Generation EU & PNRR, Italy) under the SPOKE 8: Platform for DNA/RNA delivery project. The authors thank Valentina Giudice and Alexandra Correia for their technical support. The authors thank Behnam Lak and Kiran Ahmad (University of Helsinki) for technical assistance with cryo-EM. The facilities and expertise of the HiLIFE Cryo-EM unit at the University of Helsinki, a member of Instruct-ERIC Centre Finland, FINStruct, and Biocenter Finland are acknowledged. Prof. Della Porta acknowledges financial support from University of Salerno Research Funds (FARB 2023). Prof. Santos acknowledges financial support from UMCG Research Funds.

References

1. Riley G. The pathogenesis of tendinopathy. A molecular perspective. Rheumatology [Internet]. 2004 Feb 1 [cited 2024 Oct 20];43(2):131–42. Available from: https://dx.doi.org/10.1093/rheumatology/keg448
2. Canosa-Carro L, Bravo-Aguilar M, Abuín-Porras V, Almazán-Polo J, García-Pérez-de-Sevilla G, Rodríguez-Costa I, et al. Current understanding of the diagnosis and management of the tendinopathy: An update from the lab to the clinical practice. Disease-a-Month [Internet]. 2022;68(10):101314. Available from: https://www.sciencedirect.com/science/article/pii/S0011502921001905
3. Freedman BR, Kuttler A, Beckmann N, Nam S, Kent D, Schuleit M, et al. Enhanced tendon healing by a tough hydrogel with an adhesive side and high drug-loading capacity. Nature Biomedical Engineering 2022 [Internet]. 2022 Jan 3 [cited 2022 Jan 5];1–13. Available from: https://www.nature.com/articles/s41551-021-00810-0
4. Maffulli N, Longo UG, Loppini M, Denaro V. Current treatment options for tendinopathy. Expert Opin Pharmacother [Internet]. 2010 Sep [cited 2024 Jul 29];11(13):2177–86. Available from: https://www.tandfonline.com/doi/abs/10.1517/14656566.2010.495715
5. Maffulli N, Cuozzo F, Migliorini F, Oliva F. The tendon unit: biochemical, biomechanical, hormonal influences. Journal of Orthopaedic Surgery and Research 2023 18:1 [Internet]. 2023 Apr 21 [cited 2024 Jul 29];18(1):1–9. Available from: https://josr-online.biomedcentral.com/articles/10.1186/s13018-023-03796-4
6. Li Y, Wu T, Liu S. Identification and Distinction of Tenocytes and Tendon-Derived Stem Cells. Front Cell Dev Biol [Internet]. 2021 Apr 16 [cited 2024 Oct 21];9:629515. Available from: www.frontiersin.org
7. Bi Y, Ehirchiou D, Kilts TM, Inkson CA, Embree MC, Sonoyama W, et al. Identification of tendon stem/progenitor cells and the role of the extracellular matrix in their niche. Nature Medicine 2007 13:10 [Internet]. 2007 Sep 9 [cited 2024 Oct 21];13(10):1219–27. Available from: https://www.nature.com/articles/nm1630
8. Huang Z, Yin Z, Xu J, Fei Y, Heng BC, Jiang X, et al. Tendon Stem/Progenitor Cell Subpopulations and Their Implications in

Tendon Biology. Front Cell Dev Biol [Internet]. 2021 Feb 18 [cited 2024 Oct 21];9:631272. Available from: www.frontiersin.org

9. Ciardulli MC, Scala P, Giudice V, Santoro A, Selleri C, Oliva F, et al. Stem Cells from Healthy and Tendinopathic Human Tendons: Morphology, Collagen and Cytokines Expression and Their Response to T3 Thyroid Hormone. Cells [Internet]. 2022 Aug 1 [cited 2024 Jul 17];11(16):2545. Available from: https://www.mdpi.com/2073-4409/11/16/2545/htm
10. Lei T, Zhang T, Ju W, Chen X, Heng BC, Shen W, et al. Biomimetic strategies for tendon/ligament-to-bone interface regeneration. Bioact Mater [Internet]. 2021;6(8):2491–510. Available from: https://www.sciencedirect.com/science/article/pii/S2452199X21000359
11. Quintero D, Perucca Orfei C, Kaplan LD, de Girolamo L, Best TM, Kouroupis D. The roles and therapeutic potentialof mesenchymal stem/stromal cells and their extracellular vesicles in tendinopathies. Front Bioeng Biotechnol [Internet]. 2023;11. Available from: https://www.frontiersin.org/articles/10.3389/fbioe.2023.1040762
12. Doyle LM, Wang MZ. Overview of Extracellular Vesicles, Their Origin, Composition, Purpose, and Methods for Exosome Isolation and Analysis. Cells [Internet]. 2019;8(7). Available from: https://www.mdpi.com/2073-4409/8/7/727
13. Haraszti RA, Didiot MC, Sapp E, Leszyk J, Shaffer SA, Rockwell HE, et al. High-resolution proteomic and lipidomic analysis of exosomes and microvesicles from different cell sources. J Extracell Vesicles [Internet]. 2016;5(1):32570. Available from: https://onlinelibrary.wiley.com/doi/abs/10.3402/jev.v5.32570
14. Kar R, Dhar R, Mukherjee S, Nag S, Gorai S, Mukerjee N, et al. Exosome-Based Smart Drug Delivery Tool for Cancer Theranostics. ACS Biomater Sci Eng [Internet]. 2023 Feb 13;9(2):577–94. Available from: https://doi.org/10.1021/acsbiomaterials.2c01329
15. Zhang X, Zhang H, Gu J, Zhang J, Shi H, Qian H, et al. Engineered Extracellular Vesicles for Cancer Therapy. Advanced Materials [Internet]. 2021 Apr 1 [cited 2024 Jul 22];33(14):2005709. Available from: https://onlinelibrary.wiley.com/doi/full/10.1002/adma.202005709
16. Gopalarethinam J, Nair AP, Iyer M, Vellingiri B, Subramaniam MD. Advantages of mesenchymal stem cell over the other stem cells. Acta Histochem. 2023 May 1;125(4):152041.
17. Arifka M, Wilar G, Elamin KM, Wathoni N. Polymeric Hydrogels as Mesenchymal Stem Cell Secretome Delivery System in Biomedical Applications. Polymers (Basel) [Internet]. 2022;14(6). Available from: https://www.mdpi.com/2073-4360/14/6/1218
18. Kou M, Huang L, Yang J, Chiang Z, Chen S, Liu J, et al. Mesenchymal stem cell-derived extracellular vesicles for immunomodulation and regeneration: a next generation therapeutic tool? Cell Death Dis [Internet]. 2022;13(7):580. Available from: https://doi.org/10.1038/s41419-022-05034-x
19. González-Cubero E, González-Fernández ML, Gutiérrez-Velasco L, Navarro-Ramírez E, Villar-Suárez V. Isolation and characterization of exosomes from adipose tissue-derived mesenchymal stem cells. J Anat [Internet]. 2021;238(5):1203–17. Available from: https://onlinelibrary.wiley.com/doi/abs/10.1111/joa.13365
20. Fuloria S, Subramaniyan V, Dahiya R, Dahiya S, Sudhakar K, Kumari U, et al. Mesenchymal Stem Cell-Derived Extracellular Vesicles: Regenerative Potential and Challenges. Biology (Basel) [Internet]. 2021;10(3). Available from: https://www.mdpi.com/2079-7737/10/3/172
21. Chen Z, Jin M, He H, Dong J, Li J, Nie J, et al. Mesenchymal stem cells and macrophages and their interactions in tendon-bone healing. J Orthop Translat [Internet]. 2023;39:63–73. Available from: https://www.sciencedirect.com/science/article/pii/S2214031X22001553
22. Rayamajhi S, Nguyen TDT, Marasini R, Aryal S. Macrophage-derived exosome-mimetic hybrid vesicles for tumor targeted drug delivery. Acta Biomater. 2019 Aug 1;94:482–94.
23. van der Koog L, Gandek TB, Nagelkerke A. Liposomes and Extracellular Vesicles as Drug Delivery Systems: A Comparison of Composition, Pharmacokinetics, and Functionalization. Adv Healthc Mater [Internet]. 2022 Mar 1 [cited 2024 Oct 1];11(5):2100639. Available from: https://onlinelibrary.wiley.com/doi/full/10.1002/adhm.202100639
24. Gao H, Wang S, Liu Z, Hirvonen JT, A. Santos H. Mycophenolic Acid-loaded Naïve Macrophage-derived Extracellular Vesicles Rescue Cardiac Myoblast after Inflammatory Injury. ACS Appl Bio Mater [Internet]. 2023 Oct 16 [cited 2024 Jul 22];6(10):4269–76. Available from: https://pubs.acs.org/doi/full/10.1021/acsabm.3c00475
25. Zhang J, Ji C, Zhang H, Shi H, Mao F, Qian H, et al. Engineered neutrophil-derived exosome-like vesicles for targeted cancer therapy. Sci Adv [Internet]. 2022 Jan 1 [cited 2024 Jul 22];8(2):8207. Available from: https://www.science.org/doi/10.1126/sciadv.abj8207
26. Yong T, Zhang X, Bie N, Zhang H, Zhang X, Li F, et al. Tumor exosome-based nanoparticles are efficient drug carriers for chemotherapy. Nature Communications 2019 10:1 [Internet]. 2019 Aug 23 [cited 2024 Jul 22];10(1):1–16. Available from: https://www.nature.com/articles/s41467-019-11718-4
27. Mathew B, Acha LG, Torres LA, Huang CC, Liu A, Kalinin S, et al. MicroRNA-based engineering of mesenchymal stem cell extracellular vesicles for treatment of retinal ischemic disorders: Engineered extracellular vesiclesand retinal ischemia. Acta Biomater [Internet]. 2023;158:782–97. Available from: https://www.sciencedirect.com/science/article/pii/S1742706123000132
28. Yang Y, Mao F, Guo L, Shi J, Wu M, Cheng S, et al. Tumor cells derived-extracellular vesicles transfer miR-3129 to promote hepatocellular carcinoma metastasis by targeting TXNIP. Digestive and Liver Disease [Internet]. 2021;53(4):474–85. Available from: https://www.sciencedirect.com/science/article/pii/S1590865821000098
29. Xie C, Du LY, Guo F, Li X, Cheng B. Exosomes derived from microRNA-101-3p-overexpressing human bone marrow mesenchymal stem cells suppress oral cancer cell proliferation, invasion, and migration. Mol Cell Biochem [Internet]. 2019;458(1):11–26. Available from: https://doi.org/10.1007/s11010-019-03526-7
30. Huang X, Wu W, Jing D, Yang L, Guo H, Wang L, et al. Engineered exosome as targeted lncRNA MEG3 delivery vehicles for osteosarcoma therapy. Journal of Controlled Release [Internet]. 2022;343:107–17. Available from: https://www.sciencedirect.com/science/article/pii/S0168365922000402
31. Roerig J, Mitrach F, Schmid M, Hause G, Hacker MC, Wölk C, et al. Synergistic siRNA Loading of Extracellular Vesicles Enables Functional Delivery into Cells. Small Methods [Internet]. 2022;6(12):2201001. Available from: https://onlinelibrary.wiley.com/doi/abs/10.1002/smtd.202201001

32. Haney MJ, Klyachko NL, Harrison EB, Zhao Y, Kabanov A V, Batrakova E V. TPP1 Delivery to Lysosomes with Extracellular Vesicles and their Enhanced Brain Distribution in the Animal Model of Batten Disease. Adv Healthc Mater [Internet]. 2019;8(11):1801271. Available from: https://onlinelibrary.wiley.com/doi/abs/10.1002/adhm.201801271
33. Lamichhane TN, Jeyaram A, Patel DB, Parajuli B, Livingston NK, Arumugasaamy N, et al. Oncogene Knockdown via Active Loading of Small RNAs into Extracellular Vesicles by Sonication. Cell Mol Bioeng [Internet]. 2016;9(3):315–24. Available from: https://doi.org/10.1007/s12195-016-0457-4
34. Liu H, Huang L, Mao M, Ding J, Wu G, Fan W, et al. Viral Protein-Pseudotyped and siRNA-Electroporated Extracellular Vesicles for Cancer Immunotherapy. Adv Funct Mater [Internet]. 2020;30(52):2006515. Available from: https://onlinelibrary.wiley.com/doi/abs/10.1002/adfm.202006515
35. Rong Y, Wang Z, Tang P, Wang J, Ji C, Chang J, et al. Engineered extracellular vesicles for delivery of siRNA promoting targeted repair of traumatic spinal cord injury. Bioact Mater [Internet]. 2023;23:328–42. Available from: https://www.sciencedirect.com/science/article/pii/S2452199X22004753
36. Geng Y, Long X, Zhang Y, Wang Y, You G, Guo W, et al. FTO-targeted siRNA delivery by MSC-derived exosomes synergistically alleviates dopaminergic neuronal death in Parkinson's disease via m6A-dependent regulation of ATM mRNA. J Transl Med [Internet]. 2023;21(1):652. Available from: https://doi.org/10.1186/s12967-023-04461-4
37. Rhim WK, Kim JY, Lee SY, Cha SG, Park JM, Park HJ, et al. Recent advances in extracellular vesicle engineering and its applications to regenerative medicine. Biomater Res [Internet]. 2023 Dec 1 [cited 2024 Oct 2];27(1):130. Available from: https://spj.science.org/doi/10.1186/s40824-023-00468-6
38. Rajana N, Mounika A, Chary PS, Bhavana V, Urati A, Khatri D, et al. Multifunctional hybrid nanoparticles in diagnosis and therapy of breast cancer. Journal of Controlled Release [Internet]. 2022;352:1024–47. Available from: https://www.sciencedirect.com/science/article/pii/S0168365922007532
39. Zhao Y, Li A, Jiang L, Gu Y, Liu J. Hybrid Membrane-Coated Biomimetic Nanoparticles (HM@BNPs): A Multifunctional Nanomaterial for Biomedical Applications. Biomacromolecules [Internet]. 2021 Aug 9;22(8):3149–67. Available from: https://doi.org/10.1021/acs.biomac.1c00440
40. López-Cerdá S, Molinaro G, Rubén §, Tello P, Correia A, Waris E, et al. Antifibrotic and Pro-regenerative Effects of SMAD3 siRNA and Collagen I mRNA-Loaded Lipid Nanoparticles in Human Tenocytes. ACS Appl Nano Mater [Internet]. 2024 Jul 18 [cited 2024 Jul 22]; Available from: https://pubs.acs.org/doi/full/10.1021/acsanm.4c02996
41. López Cerdá S, Fontana F, Wang S, Correia A, Molinaro G, Pareja Tello R, et al. Development of siRNA and Budesonide Dual-Loaded Hybrid Lipid–Polymer Nanoparticles by Microfluidics Technology as a Platform for Dual Drug Delivery to Macrophages: An In Vitro Mechanistic Study. Adv Ther (Weinh) [Internet]. 2023 Aug 1 [cited 2024 Jul 22];6(8):2300048. Available from: https://onlinelibrary.wiley.com/doi/full/10.1002/adtp.202300048
42. Tramontano C, Martins JP, De Stefano L, Kemell M, Correia A, Terracciano M, et al. Microfluidic-Assisted Production of Gastro-Resistant Active-Targeted Diatomite Nanoparticles for the Local Release of Galunisertib in Metastatic Colorectal Cancer Cells. Adv Healthc Mater [Internet]. n/a(n/a):2202672. Available from: https://onlinelibrary.wiley.com/doi/abs/10.1002/adhm.202202672
43. Liu D, Zhang H, Fontana F, Hirvonen JT, Santos HA. Microfluidic-assisted fabrication of carriers for controlled drug delivery. Lab Chip [Internet]. 2017 May 31 [cited 2024 Sep 30];17(11):1856–83. Available from: https://pubs.rsc.org/en/content/articlehtml/2017/lc/c7lc00242d
44. Fondaj D, Arduino I, Lopedota AA, Denora N, Iacobazzi RM. Exploring the Microfluidic Production of Biomimetic Hybrid Nanoparticles and Their Pharmaceutical Applications. Pharmaceutics [Internet]. 2023;15(7). Available from: https://www.mdpi.com/1999-4923/15/7/1953
45. Liu C, Zhang W, Li Y, Chang J, Tian F, Zhao F, et al. Microfluidic Sonication To Assemble Exosome Membrane-Coated Nanoparticles for Immune Evasion-Mediated Targeting. Nano Lett [Internet]. 2019 Nov 13;19(11):7836–44. Available from: https://doi.org/10.1021/acs.nanolett.9b02841
46. Piffoux M, Silva AKA, Wilhelm C, Gazeau F, Tareste D. Modification of Extracellular Vesicles by Fusion with Liposomes for the Design of Personalized Biogenic Drug Delivery Systems. ACS Nano [Internet]. 2018 Jul 24;12(7):6830–42. Available from: https://doi.org/10.1021/acsnano.8b02053
47. Scott BL, Van Komen JS, Liu S, Weber T, Melia TJ, McNew JA. Liposome Fusion Assay to Monitor Intracellular Membrane Fusion Machines. In: Liposomes, Part B [Internet]. Academic Press; 2003. p. 274–300. (Methods in Enzymology; vol. 372). Available from: https://www.sciencedirect.com/science/article/pii/S0076687903720163
48. Mondal J, Pillarisetti S, Junnuthula V, Saha M, Hwang SR, Park I kyu, et al. Hybrid exosomes, exosome-like nanovesicles and engineered exosomes for therapeutic applications. Journal of Controlled Release. 2023 Jan 1;353:1127–49.
49. Chan MH, Chang ZX, Huang CYF, Lee LJ, Liu RS, Hsiao M. Integrated therapy platform of exosomal system: hybrid inorganic/organic nanoparticles with exosomes for cancer treatment. Nanoscale Horiz [Internet]. 2022 Mar 28 [cited 2024 Jul 11];7(4):352–67. Available from: https://pubs.rsc.org/en/content/articlehtml/2022/nh/d1nh00637a
50. Lv Q, Cheng L, Lu Y, Zhang X, Wang Y, Deng J, et al. Thermosensitive Exosome–Liposome Hybrid Nanoparticle-Mediated Chemoimmunotherapy for Improved Treatment of Metastatic Peritoneal Cancer. Advanced Science [Internet]. 2020 Sep 1 [cited 2024 Jul 11];7(18):2000515. Available from: https://onlinelibrary.wiley.com/doi/full/10.1002/advs.202000515
51. Jürgens DC, Deßloch L, Porras-Gonzalez D, Winkeljann J, Zielinski S, Munschauer M, et al. Lab-scale siRNA and mRNA LNP manufacturing by various microfluidic mixing techniques – an evaluation of particle properties and efficiency. OpenNano. 2023 Jul 1;12:100161.
52. O'Brien Laramy MN, Costa AP, Cebrero YM, Joseph J, Sarode A, Zang N, et al. Process Robustness in Lipid Nanoparticle Production: A Comparison of Microfluidic and Turbulent Jet Mixing. Mol Pharm [Internet]. 2023 Aug 7;20(8):4285–96. Available from: https://doi.org/10.1021/acs.molpharmaceut.3c00390
53. Boufi S, Bel Haaj S, Magnin A, Pignon F, Impéror-Clerc M, Mortha G. Ultrasonic assisted production of starch nanoparticles: Structural characterization and mechanism of disintegration. Ultrason Sonochem. 2018 Mar 1;41:327–36.

54. Evers MJW, van de Wakker SI, de Groot EM, de Jong OG, Gitz-François JJJ, Seinen CS, et al. Functional siRNA Delivery by Extracellular Vesicle–Liposome Hybrid Nanoparticles. Adv Healthc Mater [Internet]. 2022;11(5):2101202. Available from: https://onlinelibrary.wiley.com/doi/abs/10.1002/adhm.202101202

55. Han Z, Lv W, Li Y, Chang J, Zhang W, Liu C, et al. Improving Tumor Targeting of Exosomal Membrane-Coated Polymeric Nanoparticles by Conjugation with Aptamers. ACS Appl Bio Mater [Internet]. 2020 May 18;3(5):2666–73. Available from: https://doi.org/10.1021/acsabm.0c00181

56. Gonzalez-Rodriguez D, Guillou L, Cornat F, Lafaurie-Janvore J, Babataheri A, de Langre E, et al. Mechanical Criterion for the Rupture of a Cell Membrane under Compression. Biophys J. 2016 Dec 20;111(12):2711–21.

57. Tan SCW, Yang T, Gong Y, Liao K. Rupture of plasma membrane under tension. J Biomech [Internet]. 2011;44(7):1361–6. Available from: https://www.sciencedirect.com/science/article/pii/S0021929011000376

58. Hategan A, Law R, Kahn S, Discher DE. Adhesively-Tensed Cell Membranes: Lysis Kinetics and Atomic Force Microscopy Probing. Biophys J [Internet]. 2003;85(4):2746–59. Available from: https://www.sciencedirect.com/science/article/pii/S0006349503746979

59. Xie X, Xu AM, Angle MR, Tayebi N, Verma P, Melosh NA. Mechanical Model of Vertical Nanowire Cell Penetration. Nano Lett [Internet]. 2013 Dec 11;13(12):6002–8. Available from: https://doi.org/10.1021/nl403201a

60. Nair A, Javius-Jones K, Bugno J, Poellmann MJ, Mamidi N, Kim IS, et al. Hybrid Nanoparticle System Integrating Tumor-Derived Exosomes and Poly(amidoamine) Dendrimers: Implications for an Effective Gene Delivery Platform. Chemistry of Materials [Internet]. 2023 Apr 25;35(8):3138–50. Available from: https://doi.org/10.1021/acs.chemmater.2c03705

61. Hu S, Wang X, Li Z, Zhu D, Cores J, Wang Z, et al. Platelet membrane and stem cell exosome hybrids enhance cellular uptake and targeting to heart injury. Nano Today [Internet]. 2021;39:101210. Available from: https://www.sciencedirect.com/science/article/pii/S1748013221001353

62. Lamparelli EP, Ciardulli MC, Scala P, Scognamiglio M, Charlier B, Di Pietro P, et al. Lipid nano-vesicles for thyroid hormone encapsulation: A comparison between different fabrication technologies, drug loading, and an in vitro delivery to human tendon stem/progenitor cells in 2D and 3D culture. Int J Pharm [Internet]. 2022;624:122007. Available from: https://www.sciencedirect.com/science/article/pii/S0378517322005622

63. Kulkarni JA, Darjuan MM, Mercer JE, Chen S, van der Meel R, Thewalt JL, et al. On the Formation and Morphology of Lipid Nanoparticles Containing Ionizable Cationic Lipids and siRNA. ACS Nano [Internet]. 2018 May 22;12(5):4787–95. Available from: https://doi.org/10.1021/acsnano.8b01516

64. Eygeris Y, Patel S, Jozic A, Sahay G. Deconvoluting Lipid Nanoparticle Structure for Messenger RNA Delivery. Nano Lett [Internet]. 2020 Jun 10;20(6):4543–9. Available from: https://doi.org/10.1021/acs.nanolett.0c01386

65. Sato YT, Umezaki K, Sawada S, Mukai S atsu, Sasaki Y, Harada N, et al. Engineering hybrid exosomes by membrane fusion with liposomes. Sci Rep [Internet]. 2016;6(1):21933. Available from: https://doi.org/10.1038/srep21933

66. Ding Z, Greenberg ZF, Serafim MF, Ali S, Jamieson JC, Traktuev DO, et al. Understanding molecular characteristics of extracellular vesicles derived from different types of mesenchymal stem cells for therapeutic translation. Extracellular Vesicle [Internet]. 2024;3:100034. Available from: https://www.sciencedirect.com/science/article/pii/S2773041724000015

67. Zhao H, Shang Q, Pan Z, Bai Y, Li Z, Zhang H, et al. Exosomes From Adipose-Derived Stem Cells Attenuate Adipose Inflammation and Obesity Through Polarizing M2 Macrophages and Beiging in White Adipose Tissue. Diabetes [Internet]. 2017 Nov 13;67(2):235–47. Available from: https://doi.org/10.2337/db17-0356

68. Pogozhykh O, Pogozhykh D, Neehus AL, Hoffmann A, Blasczyk R, Müller T. Molecular and cellular characteristics of human and non-human primate multipotent stromal cells from the amnion and bone marrow during long term culture. Stem Cell Res Ther [Internet]. 2015;6(1):150. Available from: https://doi.org/10.1186/s13287-015-0146-6

69. Molinaro G, Fontana F, Pareja Tello R, Wang S, López Cérda S, Torrieri G, et al. In Vitro Study of the Anti-inflammatory and Antifibrotic Activity of Tannic Acid-Coated Curcumin-Loaded Nanoparticles in Human Tenocytes. ACS Appl Mater Interfaces [Internet]. 2023 May 17;15(19):23012–23. Available from: https://doi.org/10.1021/acsami.3c05322

70. Fontana F, Molinaro G, Moroni S, Pallozzi G, Ferreira MPA, Tello RP, et al. Biomimetic Platelet-Cloaked Nanoparticles for the Delivery of Anti-Inflammatory Curcumin in the Treatment of Atherosclerosis. Adv Healthc Mater [Internet]. n/a(n/a):2302074. Available from: https://onlinelibrary.wiley.com/doi/abs/10.1002/adhm.202302074

71. Lu J, Chen H, Lyu K, Jiang L, Chen Y, Long L, et al. The Functions and Mechanisms of Tendon Stem/Progenitor Cells in Tendon Healing. Stem Cells Int [Internet]. 2023 Jan 1 [cited 2024 Jul 17];2023(1):1258024. Available from: https://onlinelibrary.wiley.com/doi/full/10.1155/2023/1258024

72. Zhang C, Zhu J, Zhou Y, Thampatty BP, Wang JHC. Tendon Stem/Progenitor Cells and Their Interactions with Extracellular Matrix and Mechanical Loading. Stem Cells Int [Internet]. 2019 Jan 1 [cited 2024 Jul 17];2019(1):3674647. Available from: https://onlinelibrary.wiley.com/doi/full/10.1155/2019/3674647

73. Millar NL, Silbernagel KG, Thorborg K, Kirwan PD, Galatz LM, Abrams GD, et al. Tendinopathy. Nat Rev Dis Primers [Internet]. 2021;7(1):1. Available from: https://doi.org/10.1038/s41572-020-00234-1

74. Walia B, Huang AH. Tendon stem progenitor cells: Understanding the biology to inform therapeutic strategies for tendon repair. Journal of Orthopaedic Research® [Internet]. 2019 Jun 1 [cited 2024 Jul 17];37(6):1270–80. Available from: https://onlinelibrary.wiley.com/doi/full/10.1002/jor.24156

75. Huisman E, Lu A, McCormack RG, Scott A. Enhanced collagen type i synthesis by human tenocytes subjected to periodic in vitro mechanical stimulation. BMC Musculoskelet Disord [Internet]. 2014 Nov 21 [cited 2024 Jul 17];15(1):1–8. Available from: https://bmcmusculoskeletdisord.biomedcentral.com/articles/10.1186/1471-2474-15-386

76. Yu H, Cheng J, Shi W, Ren B, Zhao F, Shi Y, et al. Bone marrow mesenchymal stem cell-derived exosomes promote tendon regeneration by facilitating the proliferation and migration of

endogenous tendon stem/progenitor cells. Acta Biomater. 2020 Apr 1;106:328–41.

77. Wang Y, He G, Guo Y, Tang H, Shi Y, Bian X, et al. Exosomes from tendon stem cells promote injury tendon healing through balancing synthesis and degradation of the tendon extracellular matrix. J Cell Mol Med [Internet]. 2019 Aug 1 [cited 2024 Jul 17];23(8):5475–85. Available from: https://onlinelibrary.wiley.com/doi/full/10.1111/jcmm.14430
78. Gomez-Florit M, Labrador-Rached CJ, Domingues RMA, Gomes ME. The tendon microenvironment: Engineered in vitro models to study cellular crosstalk. Adv Drug Deliv Rev. 2022 Jun 1;185:114299.
79. Herchenhan A, Bayer ML, Eliasson P, Magnusson SP, Kjaer M. Insulin-like growth factor I enhances collagen synthesis in engineered human tendon tissue. Growth Hormone & IGF Research. 2015 Feb 1;25(1):13–9.
80. Xia W, Szomor Z, Wang Y, Murrell GAC. Nitric oxide enhances collagen synthesis in cultured human tendon cells. Journal of Orthopaedic Research [Internet]. 2006 Feb 1 [cited 2024 Jul 22];24(2):159–72. Available from: https://onlinelibrary.wiley.com/doi/full/10.1002/jor.20060
81. Barnes AM, Ashok A, Makareeva EN, Brusel M, Cabral WA, Weis MA, et al. COL1A1 C-propeptide mutations cause ER mislocalization of procollagen and impair C-terminal procollagen processing. Biochimica et Biophysica Acta (BBA) - Molecular Basis of Disease. 2019 Sep 1;1865(9):2210–23.
82. Fratzl P. Collagen: Structure and Mechanics, an Introduction. Collagen: Structure and Mechanics [Internet]. 2008 [cited 2024 Jul 17];1–13. Available from: https://link.springer.com/chapter/10.1007/978-0-387-73906-9_1
83. Mienaltowski MJ, Birk • D E, Mienaltowski MJ, Birk DE. Structure, Physiology, and Biochemistry of Collagens. Adv Exp Med Biol [Internet]. 2014 [cited 2024 Jul 17];802:5–29. Available from: https://link.springer.com/chapter/10.1007/978-94-007-7893-1_2
84. Saggese G, Bertelloni S, Baroncelli GI, Di Nero G. Serum levels of carboxyterminal propeptide of type I procollagen in healthy children from 1 st year of life to adulthood and in metabolic bone diseases. Eur J Pediatr [Internet]. 1992;151(10):764–8. Available from: https://doi.org/10.1007/BF01959087
85. Parfitt AM, Simon LS, Villanueva AR, Krane SM. Procollagen type I carboxy-terminal extension peptide in serum as a marker of collagen biosynthesis in bone. Correlation with iliac bone formation rates and comparison with total alkaline phosphatase. Journal of Bone and Mineral Research [Internet]. 1987 Oct 1;2(5):427–36. Available from: https://doi.org/10.1002/jbmr.5650020510
86. Seo WY, Kim JH, Baek DS, Kim SJ, Kang S, Yang WS, et al. Production of recombinant human procollagen type I C-terminal propeptide and establishment of a sandwich ELISA for quantification. Scientific Reports 2017 7:1 [Internet]. 2017 Nov 21 [cited 2024 Jul 17];7(1):1–13. Available from: https://www.nature.com/articles/s41598-017-16290-9
87. Luo LF, Shi Y, Zhou Q, Xu SZ, Lei TC. Insufficient expression of the melanocortin-1 receptor by human dermal fibroblasts contributes to excess collagen synthesis in keloid scars. Exp Dermatol [Internet]. 2013;22(11):764–6. Available from: https://onlinelibrary.wiley.com/doi/abs/10.1111/exd.12250
88. Chamberlain CS, Kink JA, Wildenauer LA, McCaughey M, Henry K, Spiker AM, et al. Exosome-educated macrophages and exosomes differentially improve ligament healing. Stem Cells [Internet]. 2021 Jan 1 [cited 2024 Jul 17];39(1):55–61. Available from: https://dx.doi.org/10.1002/stem.3291
89. Costa-Almeida R, Calejo I, Reis RL, Gomes ME. Crosstalk between adipose stem cells and tendon cells reveals a temporal regulation of tenogenesis by matrix deposition and remodeling. J Cell Physiol [Internet]. 2018 Jul 1 [cited 2024 Jul 17];233(7):5383–95. Available from: https://onlinelibrary.wiley.com/doi/full/10.1002/jcp.26363

Data availability statement

View Article Online
DOI: 10.1039/D4BM01405G

Data for this article are available at the Zenodo repository at https://zenodo.org/